Microfabricated Optically Pumped Gradiometer with Uniform Buffer Gases

Austin R. Parrish*, Radwan Noor*†, and Andrei M. Shkel*
Email: {aparrish, andrei.shkel} @ uci.edu rnoor@kacst.edu.sa
*Department of Mechanical and Aerospace Engineering, University of California - Irvine, Irvine, CA, USA
†King Abdulaziz City for Science and Technology (KACST), Riyadh, Saudi Arabia

***Abstract*—This paper reports on the development of a microfabricated gradiometer that permits uniform buffer gas content in both magnetometers. This improves the common mode noise rejection of the gradiometer by ensuring the broadening and shift of the Rb optical absorption line are uniform. The reported fabrication process permits micro-channels connecting the two magnetometers allowing for uniform buffer gas pressure. We discuss two methods of characterizing the common mode rejection ratio (CMRR), before and after measuring the frequency response of the individual magnetometers. The average uncalibrated and calibrated CMRR achieved in a table-top setup was 72.7 and 85.0 respectively over a bandwidth 3-200Hz.**

Keywords—atomic sensors, microfabrication, magnetometer, gradiometer, common mode noise rejection

I. Introduction

Magnetometers are widely used in navigation to find the direction of the Earth's magnetic field, thus used as a reference for orienting the inertial measurement unit. It is also possible to use spatial variations in the Earth's magnetic field (due to remnant magnetization of the Earth's crust) as a reference for magnetic navigation [1]. However, the magnetic field of the Earth is subject to temporal effects primarily due to current in the ionosphere, which is greater in the event of solar wind. The use of a gradiometer eliminates temporal effects as the spatial gradient for temporal variations is nearly zero [2].

Gradiometers permit rejection of common mode noise in magnetometers, particularly improving operation in environments with large ambient magnetic background. If the magnetometer cells were filled with different buffer gas pressures, the Rb atoms would experience different shifts and broadening of the optical absorption line. This reduces the common mode noise rejection in the gradiometer [3]. The presented design permits uniform buffer gas pressure between the two atomic magnetometers. While multi-channel gradiometers using one cell have been implemented, to our knowledge, only one microfabricated gradiometer capable of multi-axis pumping and probing has been reported [4].

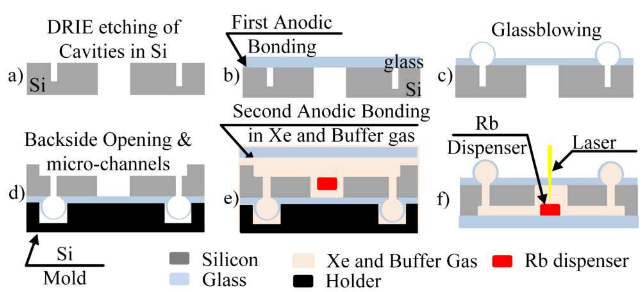

Fig. 1 Description of process flow: (a) DRIE etching of 900µm and through wafer cavities, (b) first anodic bonding of glass to the etched Si wafer, (c) glassblowing of cells, (d) cell back-side opening and channel definition using DRIE etching, (e) loading Rb dispenser and second anodic bonding in environment of Xe and buffer gases, and (f) dispensing alkali metal through microchannel by laser heating of Rb source.

This work was partially funded by the Agency for Defense Development (ADD). The work of R. M. Noor was supported by King Abdulaziz City for Science and Technology (KACST).

II. Design and Fabrication

The fabrication process, as introduced in [5], is shown in Fig. 1 and begins by etching 900µm and through-wafer cavities in a 1mm thick Si wafer, Fig. 1(a). Next, anodic bonding seals the etched cavities under atmospheric pressure, Fig. 1(b). The wafer-stack is then placed in a furnace at 850˚C for 5-7 minutes, forming into spherically shaped shells due to trapped air inside the cavities, Fig. 1(c). Following, 100µm deep channels are etched into backside of the Si wafer using DRIE etching, Fig. 1(d). A second anodic bonding is performed to install a Rb dispenser pill in an environment of 85 Torr Xe, 45 Torr Ne, and 305 Torr N_2, Fig. 1(e). Finally, the Rb is dispensed by heating the dispenser pill using laser heating, Fig. 1(f). The two glassblown cells are separated by a distance of 5.5mm and each are probed as magnetometers in this experiment.

III. Gradiometer Implementation and Characterization

A. Gradiometer Implementation

The table-top gradiometer implementation is shown in Fig. 2. The gradiometer is housed in a µ-metal shield with integrated 3-axis magnetic field coils (D = 6in) and a miniaturized oven made from thermal insulating material. A laser with optical power 4W is used to heat the cells to a temperature of 140˚C. The pump beam is oriented along the z-axis, circularly polarized, and locked to the Rb D1 line (795nm). The probe beam is oriented along the y-axis, linearly polarized, and slightly detuned from the Rb D2 line (780nm). A DC field of 2.5µT and an RF field of 13kHz with an amplitude of 10.5µTpp were applied along the z-axis. The magnetometer operates by detecting the projection of the polarization along the y-axis via Faraday rotation of the probe beam. The RF field was used as a reference for the lock-in amplifier to demodulate the output of the Faraday detector. Though the cells contain both Rb and Xe and are therefore capable of nuclear magnetic resonance operation, the implementation discussed in this paper is purely a Rb magnetometer.

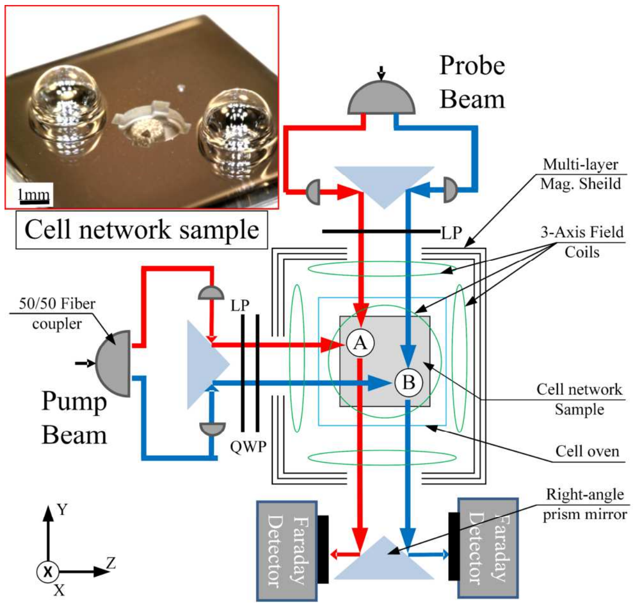

Fig. 2 Gradiometer implementation. (LP: linear polarizer, QWP: quarter wave plate, Faraday detector: balanced polarimeter to detect Faraday rotation)

B. *Magnetometer Characterization*

The frequency response of each magnetometer was characterized by applying a calibration field of amplitude 35nTpp with varying frequency swept from 3 to 200 Hz along the y-axis similar to the process described in [6]. This calibration accounts for the mismatch in phase and relative gain between the two magnetometers. While the buffer gases in both magnetometers are identical, the alignment of the pump and probe beams accounts for the disparity in the frequency response of the two magnetometers. The frequency response of each magnetometer is reported in Fig. 3(a,b). The peaks at 8.8Hz and 29.5Hz are due to the presence of ^{131}Xe and ^{129}Xe and correspond to their Larmor frequency in the presence of the 2.5μT DC field. The measured sensitivity of the magnetometers is roughly 10pT/√Hz from 3-100Hz.

IV. Experimental Results

The common mode rejection ratio (CMRR) of the gradiometer was measured by applying digitally synthesized magnetic noise with RMS amplitude of 70nT along the y-axis of the setup. Two definitions of the common mode rejection ratio are given in Eq's (1,2). B is the magnetic field reading of the magnetometers and is defined as $B = S/M$, where S is the raw output of the magnetometer and M is the calibrated frequency response of each magnetometer. The uncalibrated CMRR in Eq. (1) [6] quantifies the matching of the relative gain and phase of the two magnetometers. The gradiometer output (G), however, corresponds to the calibrated response of each magnetometer $G = B_1 - B_2$. We use an alternative definition of CMRR, defined by Eq. (2), to describe the common mode noise rejection of the calibrated gradiometer output. The average uncalibrated CMRR was recorded as 72.7 and the average calibrated CMRR was recorded as 85.0 over the 3-200Hz bandwidth.

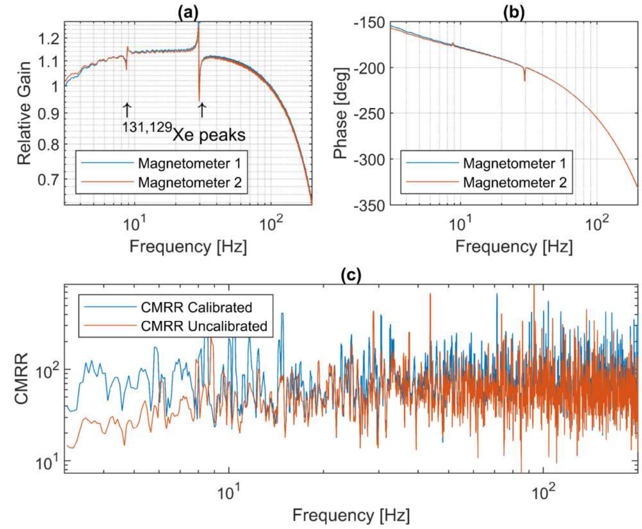

Fig. 3 Magnetometer and gradiometer characterization: (a,b) describe the relative gain (a) and phase (b) of the frequency response of magnetometers derived from calibration. (c) shows the measured CMRR (data shown in (c) is a moving average of 5 samples).

$$CMRR_{Uncalibrated} = \frac{M_1B_1+M_2B_2}{2(M_1B_1-M_2B_2)} = \frac{S_1+S_2}{2(S_1-S_2)} \quad (1)$$

$$CMRR_{Calibrated} = \frac{B_1+B_2}{2(B_1-B_2)} \quad (2)$$

V. Conclusion

We have described a microfabricated gradiometer that permits uniform buffer gas content in both magnetometers. Additionally, we described the frequency response of the magnetometers and the resulting calibrated and uncalibrated CMRR. Future work will include an analysis of the closed-loop implementation and the use of the already present Xe in a nuclear magnetic resonance (NMR) gradiometer.

Acknowledgment

Devices were designed at the UCI Microsystems Laboratory and fabricated at the UCI INRF cleanroom facility.

References

[1] A. Canciani and J. Raquet, "Airborne Magnetic Anomaly Navigation," IEEE Trans. Aerosp. Electron. Syst., vol. 53, no. 1, pp. 67–80, 2017.

[2] L. Mount, "Navigation using Vector and Tensor Measurements of the Earth's Magnetic Anomaly Field," Air Force Institute of Technology, 2018.

[3] D. Sheng, A. R. Perry, S. P. Krzyzewski, S. Geller, J. Kitching, and S. Knappe, "A microfabricated optically-pumped magnetic gradiometer," Appl. Phys. Lett., vol. 110, no. 3, p. 031106, 2017.

[4] Y. Ji, J. Shang, J. Zhang, and G. Li, "Magnetic Gradient Measurement Using Micro-Fabricated Shaped Rubidium Vapor Cell," IEEE Trans. Magn., vol. 55, no. 9, 2019, doi: 10.1109/tmag.2019.2916311

[5] R. M. Noor, N. Kulachenkov, M. H. Asadian, and A. M. Shkel, "Study on MEMS Glassblown Cells for NMR Sensors," in 2019 IEEE International Symposium on Inertial Sensors and Systems (INERTIAL), 2019.

[6] I. A. Sulai, Z. J. Deland, M. D. Bulatowicz, C. P. Wahl, R. T. Wakai, and T. G. Walker, "Characterizing atomic magnetic gradiometers for fetal magnetocardiography," Rev. Sci. Instrum., vol. 90, no. 8, pp. 1–11, 202